

Out-of-time-order correlation and detection of phase structure in Floquet transverse Ising spin system

Rohit Kumar Shukla,^{*} Gautam Kamalakar Naik,[†] and Sunil Kumar Mishra[‡]

Department of Physics, Indian Institute of Technology (Banaras Hindu University), Varanasi - 221005, India

(Dated: February 17, 2020)

We study the out-of-time-order correlation (OTOC) of the Floquet transverse Ising model and use it to verify the phase diagram of the system. First, we present the exact analytical solution of the transverse magnetization OTOC using the Jordan-Wigner transformation. In order to get the phase structure of the Floquet transverse Ising system, we use the longitudinal magnetization OTOC as it is known to serve as an order parameter of the system. We show the phase structure numerically in the transverse Ising Floquet system by using the long time average of the longitudinal magnetization OTOC. In both the open and the closed chain systems, we find distinct phases out of which two are paramagnetic (0-paramagnetic and π -paramagnetic), and two are ferromagnetic (0-ferromagnetic and π -ferromagnetic) as defined in the literature.

I. INTRODUCTION

In the last two decades, out-of-time-order correlation (OTOC) has gained a lot of attention among the researchers of various fields. One field of interest is the butterfly effects in quantum chaotic systems [1–4]. Other directions are quantum information scrambling [2, 5–13] and many-body localization [14]. The nontrivial OTOC as a holographic tool has been instrumental in determining the interplay of scrambling and entanglement [15, 16]. Many experiments have been done to measure OTOCs in various systems, *e. g.*, trapped-ion quantum magnets [17] and Nuclear Magnetic resonance quantum simulator [18].

In addition to the above fields of interest, the OTOCs are useful in determining phases of the quantum critical systems [19–21]. The phase structures of quantum critical systems have been studied extensively in the last few decades [19, 20, 22–33]. One of the simplest models to display and analyze the quantum phase transition is one dimensional transverse Ising model which is given by Hamiltonian $H = J \sum_i \sigma_i^x \sigma_{i+1}^x + h \sum_i \sigma_i^z$. This system undergoes a phase transition at $J = h$ from the ferromagnetic state ($J > h$) to the paramagnetic phase ($J < h$) [21, 34–36]. Such phase transitions in time-independent equilibrium systems have been well studied over the years. In the last few years, the OTOC has emerged as a tool to detect equilibrium and dynamical quantum phase transitions in the transverse field Ising (TFI) model and the Lipkin-Meshkov-Glick model (LMG) [21].

It has been shown that the OTOC of the ground states and quenched states can diagnose the QPTs and dynamical phase transition, respectively [21]. The ferromagnetic ($J > h$) and paramagnetic ($J < h$) phases of the transverse Ising model can be characterized by nonzero and zero long time average OTOC, respectively [21]. The pe-

riodically driven interacting quantum system known as the Floquet system, on the other hand, poses a different problem: one would expect generic Floquet systems to heat to infinite temperatures. However, specific cases of nonergodic phases with localization have been observed in Floquet systems [37, 38]. In these systems, multiple nonergodic phases with differing forms of dynamics and ordering have been observed [32].

These multiple phases are characterized by broken symmetries and topological order. In the case of transverse Ising Floquet systems, Majorana modes are produced at the ends of the long chain [25]. The zero-energy Majorana mode corresponds to the long range ferromagnetic order while the nonzero-energy Majorana mode corresponds to the paramagnetic phase [24, 25]. The sharp phase boundaries of the Floquet Ising system are explained by symmetry protected Ising order [27, 32]. For binary Floquet drive, two paramagnetic and two ferromagnetic phases can be seen in the phase diagram. The two paramagnetic/ferromagnetic phases are distinguished by the combined eigenvalues of the Floquet drives and the parity operators. On the basis of the combined eigenvalues, the paramagnetic region is divided into two parts: 0 and 0π -paramagnetic and ferromagnetic region is also divided into two parts: 0 and π -ferromagnetic [FIG. 1]. In the ferromagnetic region, all of the eigenstates have long range Ising symmetry broken order. However, in the paramagnetic phase, all of the eigenstates have long range symmetric order.

We will explore the OTOCs as a detector of phase transition in the Floquet Ising spin system. First, we will consider transverse magnetization out-of-time-order correlation (TMOTOC) and calculate the exact solution using the Jordan Wigner transformation by mapping the spin operators onto the fermionic annihilation and creation operators. Next, we will consider the longitudinal magnetization out-of-time-order correlation (LMOTOC) and explore the various phases in the Floquet Ising spin system. Our motivation is to find the phase structure of the Floquet system using a long time average of LMO-TOC.

This manuscript is organized as follows: In section II,

^{*} rohitkrshukla.rs.phy17@itbhu.ac.in

[†] gautamk.naik.phy15@itbhu.ac.in

[‡] sunilkam.app@iitbhu.ac.in

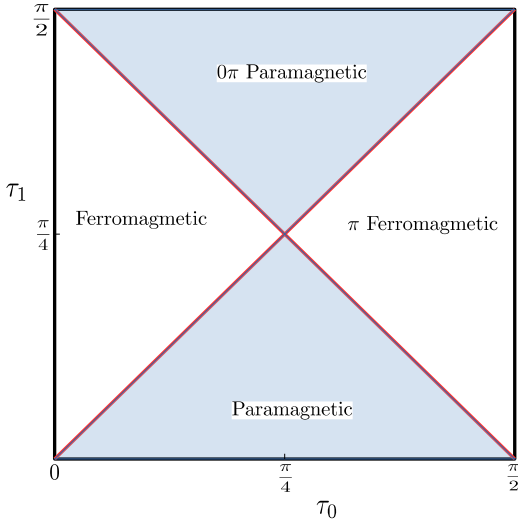


FIG. 1. Phase structure of the Floquet system with Floquet map given by eq. (1) [24, 27, 32]. There are four distinct phases in the τ_0 - τ_1 parameter space. Two of these phases, the π ferromagnetic and the 0π paramagnetic, and phases which are unique to Floquet systems.

we will discuss the model of the Floquet system. In section III, we will define the longitudinal and transverse magnetization OTOCs. We will introduce the time average of the LMOTOC for the detection of phase structures. In section III, we will discuss the various phases of the Floquet Ising system using a long time averaged LMOTOC. Subsequently, in section V, we conclude the results.

II. MODEL

We consider an integrable Floquet transverse Ising system with binary Floquet drives. The Floquet map corresponding to this system is

$$U = e^{-iH_{xx}\tau_1} e^{-iH_z\tau_0}, \quad (1)$$

where H_{xx} is the nearest neighbor Ising interaction given by $H_{xx} = \sum_{l=1}^{N-1} \sigma_l^x \sigma_{l+1}^x$ for open chain system and $H_{xx} = \sum_{l=1}^N \sigma_l^x \sigma_{l+1}^x$ for closed chain system with $\sigma_{N+1}^x = \sigma_1^x$. $H_z = \sum_{l=1}^N \sigma_l^z$ is the transverse field in z-direction. τ_0 and τ_1 are the time periods. The Hamiltonian corresponding to the above Floquet operator is:

$$H(t) = H_{xx} + \sum_{n=-\infty}^{\infty} \delta\left(n - \frac{t}{\tau_1}\right) \frac{\tau_0}{\tau_1} H_z. \quad (2)$$

III. OUT-OF-TIME-ORDER CORRELATION

The out of time order correlation (OTOC) is, in general, defined as $F(t) = \langle W(t) V W(t) V \rangle$ where V and W

are two local Hermitian operators and $W(t)$ is the Heisenberg evolution of the operator W by time t . If we consider the local operator $V = W = \sigma_l^z$, the spin operator perpendicular to the Ising axis (x-axis), we get TMOTOC, which is given by:

$$F_z(n) = \langle \phi_0 | \sigma_l^z(n) \sigma_l^z \sigma_l^z(n) \sigma_l^z | \phi_0 \rangle, \quad (3)$$

where l can take any value between 1 to N for closed spin chain. The time evolution of the spin operator at the position l after n kicks is defined as $S_l^z(n) = U^{\dagger n} S_l^z U^n$. In this case we will start with the initial state

$$|\phi_0\rangle = |\uparrow\uparrow\uparrow \cdots \uparrow\rangle, \quad (4)$$

where, $|\uparrow\rangle$ is the eigenstate of σ^z with eigenvalue $+1$. Let's consider the periodic boundary condition and even number of spins and calculate the Floquet map given by eq. (1) as;

$$U = \exp\left[-it_1 \sum_{l=1}^N S_l^x S_{l+1}^x\right] \exp\left[-it_0 \sum_{l=1}^N S_l^z\right], \quad (5)$$

where, $t_0 = 2\tau_0$, $t_1 = 4\tau_1$ and $\sigma_l^x = 2S_l^x$ gives the same unitary operator as defined in eq. (1). We calculate the analytical expression for the TMOTOC using the Jordan-Wigner transformation (for detailed calculation refer to Appendix A):

$$F_z(n) = 1 - \left(\frac{2}{N}\right)^3 \sum_{p,q,r} \left(|\Psi_r(n)|^2 \Phi_p(n)^* \Phi_q(n) - \Psi_{-p}(n) \times \Psi_r(n)^* \Phi_p(n)^* \Phi_q(n) - \Psi_q(n) \Psi_r(n)^* \Phi_p(n)^* \Phi_{-r}(n) + \Psi_q(n) \Psi_r(n)^* |\Phi_p(n)|^2 \right), \quad (6)$$

where the expansion coefficients $\Phi_q(n)$ and $\Psi_q(n)$ are defined as

$$\Phi_q(n) = |\alpha_+(q)|^2 e^{-it\gamma_q} + |\alpha_-(q)|^2 e^{it\gamma_q}, \quad (7)$$

$$\Psi_q(n) = \alpha_+(q)\beta_+(q)e^{-in\gamma_q} + \alpha_-(q)\beta_-(q)e^{in\gamma_q}. \quad (8)$$

The phase angle γ_q and the coefficients $\alpha_{\pm}(q)$ and $\beta_{\pm}(q)$ are given by

$$\cos(\gamma_q) = \cos(t_0) \cos(t_1) - \cos(q) \sin(t_0) \sin\left(\frac{t_1}{2}\right), \quad (9)$$

and

$$\alpha_{\pm}(q)^{-1} = \sqrt{1 + \left(\frac{\cos(\frac{t_1}{2}) - \cos(\gamma_q \pm t_0)}{\sin(q) \sin(t_0) \sin(\frac{t_1}{2})}\right)^2}, \quad (10)$$

$$\beta_{\pm}(q) = \alpha_{\pm}(q) \frac{\mp \sin(\gamma_q) - \cos(t_0) \cos(q) \sin(\frac{t_1}{2}) - \sin(t_0) \cos(\frac{t_1}{2})}{\sin(q) \sin(\frac{t_1}{2})} e^{-it_0}. \quad (11)$$

The allowed value of p , q and r are from $\frac{-(L-1)\pi}{L}$ to $\frac{(L-1)\pi}{L}$ differing by $\frac{2\pi}{L}$ for even number of N_F ($N_F = c_l^\dagger c_l$, Number of Fermion).

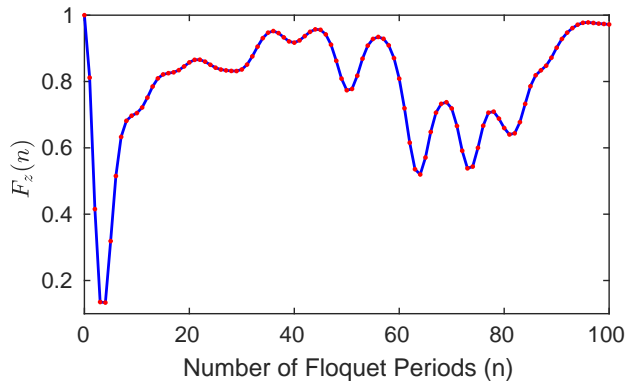


FIG. 2. $F_z(n)$ for closed chain transverse Ising Floquet system of system size $N = 12$ by using the Numerical calculations (solid line) and using the formula (point). Here we take $\tau_0 = \tau_1 = \epsilon$.

The values of $F_z(n)$ obtained by the analytical expression in eq. 6 match the values obtained numerically by exact diagonalization. For instance, for $\tau_0 = \tau_1 = \epsilon$, where $\epsilon = \frac{\pi}{28}$, we have shown the analytical and numerical results in FIG. 2. The advantage of having an easily computable formula such as eq. (6) is that we can study the TMOTOC as a function of Floquet periods τ_0 and τ_1 and see the behavior at any number of kicks. The analytical expression is of $O(L^3)$ which has a significant advantage over exact diagonalization calculations of $O(2^L)$. Inset of FIG. 3(a) shows the TMOTOC with time (kicks) using eq. 6 for system size $N = 50$ with a periodic boundary condition, where we fix $\tau_1 = \pi/24$ and $\tau_0 = \epsilon, 2\epsilon$ and 3ϵ .

The LMOTOCs have been shown to be useful in detecting the phase transitions between the paramagnetic and ferromagnetic phases in spin systems [21]. However, the same cannot be said about TMOTOC. A comparison of the behavior of the two quantities with time is shown in FIG. 3. We see from FIG. 3(a) that TMOTOCs always oscillate about a positive value for all the pairs of τ_0 and τ_1 , signaling that the long time average of TMOTOC is always a positive quantity. However, in the case of LMOTOCs, as shown in FIG. 3(b), we find that the long time average value can be either zero or a positive quantity. In order to detect the phase structure of the system, we require the order parameter characterising the distinct phases to show a sharp contrast between the phases. We see that the LMOTOCs qualify the criterion to be used as an order parameter, but TMOTOCs fail to do so.

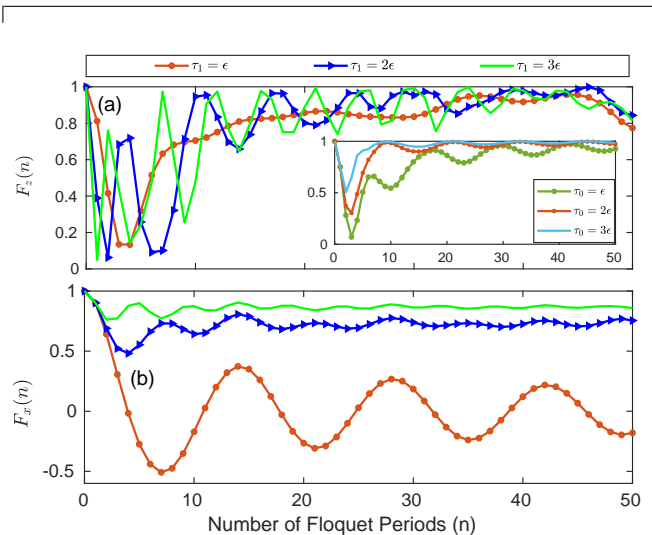


FIG. 3. (a) Variation of the real part of (a) TMOTOC and (b) LMOTOC with number of Floquet periods for a fixed $\tau_0 = \epsilon$ and $\tau_1 = \epsilon, 2\epsilon$ and 3ϵ in closed chain Floquet systems with system size $N=12$. In TMOTOC, we take the initial state as a direct product of the eigenstate of σ^z with eigenvalue $+1$. In LMOTOC, the initial state is the direct product of the eigenstate of σ^x with eigenvalue $+1$. Oscillation of the mean value of TMOTOC always remains positive value however in LMOTOC have both positive and zero value which depends on the constant value of τ_0 and τ_1 . In the inset, there is the variation of TMOTOC with the number of Floquet periods for a fixed $\tau_1 = \frac{\pi}{24}$ and $\tau_0 = \epsilon, 2\epsilon$ and 3ϵ in closed chain Floquet systems with system size $N=50$.

Upon performing a quantum quench from a polarized state, we will use the saturation value of the LMOTOC as the order parameter to distinguish between the two phases. It is calculated by numerical methods because it is not beneficial to calculate it analytically [39].

Considering $V = W = \sigma_l^x$, the spin operator along the Ising axis, we get the LMOTOC defined as:

$$F_x(n) = \langle \psi_0 | \sigma_l^x(n) \sigma_l^x \sigma_l^x(n) \sigma_l^x | \psi_0 \rangle, \quad (12)$$

We study the phase structure of the system [eq. (1)] by calculating the LMOTOC using the fully polarized initial state

$$|\psi_0\rangle = |\rightarrow \rightarrow \rightarrow \dots \rightarrow\rangle, \quad (13)$$

where, $|\rightarrow\rangle$ is the eigenstate of σ^x with eigenvalue $+1$. We consider an even number of spins in this analysis. where can take any values from $l = 1$ to N for closed spin chain and $l = \frac{N}{2}$ for open chain. $\sigma_l^x(n) = U^\dagger \sigma_l^x U^n$ is the Heisenberg evolution of σ_l^x after n Floquet periods. If the LMOTOC denoted by eq. (12) saturates to a particular value after a long period of time, this value can be

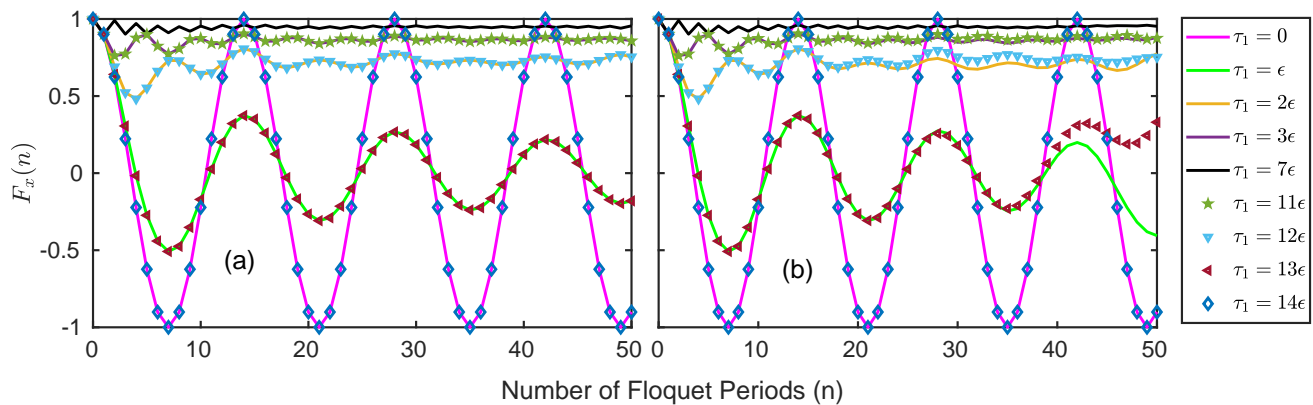


FIG. 4. Variation of the real part of LMOTOC ($F_x(n)$) with number of Floquet periods for a fixed $\tau_0 = \epsilon$ and multiple values of τ_1 in (a) closed and (b) open chain Floquet systems with system size $N=12$. The initial state is direct product of eigenstate of σ^x with eigenvalue $+1$. At $\tau_1 = 0$, $F_x(n)$ shows periodic oscillations about zero. As the value of τ_1 is increased, the $F_x(n)$ oscillates about greater non-zero values with lower amplitudes of oscillation and at $\tau_1 = \frac{\pi}{4}$, it saturates to the value 1. As increase constant value of $\tau_1 = 0$, $F_x(n)$ has same and different value as $\frac{\pi}{2} - \tau_1 = 0$ in closed and open chain respectively.

determined by taking the long time average of the LMOTOC. We define the long time-average of the LMOTOC, $\overline{F}_x(T)$ upto T Floquet periods by:

$$\overline{F}_x = \frac{1}{T} \sum_{n=1}^T F_x(n). \quad (14)$$

The long time average of the LMOTOC has a direct link with the spectral properties of the system in consideration [40]. The averaged LMOTOC links with the spectral form factor [41], a well-known quantity in random matrix theory, which is a quantifier for discreteness in the spectrum.

IV. PHASE STRUCTURE

The phase structure of the Floquet system given by eq. (1) is known to have four distinct phases in the two-dimensional parameter space of τ_0 and τ_1 . The phase diagram is shown in FIG. 1 [24, 27, 32]. Paramagnetic and ferromagnetic phases show behavior similar to their undriven counterparts. The other two of the phases observed, the π -ferromagnetic and 0π -paramagnetic are unique to Floquet systems and are not observed in undriven non-Floquet systems. The phase transitions between these phases in the τ_0 and τ_1 parameter space can be detected by calculating LMOTOCs. The LMOTOC has been shown to saturate to non-zero values in the ferromagnetic region and to zero in the paramagnetic region, at long times in the undriven systems [21]. Hence, the long time averaged LMOTOC serves as a good order parameter for paramagnetic and ferromagnetic regions in the undriven systems. In driven Floquet systems, LMOTOCs do not saturate to non-zero and zero values for all values of τ_0 and τ_1 ; we see a continuing oscillating behaviour about a non-zero or zero mean value (FIG. 4).

The time-averaged LMOTOC ($\overline{F}_x(n)$) is seen to saturate at long times in the thermodynamic limit to non-zero values in the ferromagnetic and π ferromagnetic regions, and to zero in the paramagnetic and 0π paramagnetic regions of the phase space. FIG. 5 shows the variation of the long time-average of the real part of the LMOTOC with τ_1 , for different values of τ_0 in the closed and open boundary conditions for a system size $N = 10$.

The critical points, where the phase transition occurs, are identified along the constant τ_0 line at the points where LMOTOC goes from zero to non-zero. These critical points, when mapped in the τ_0 and τ_1 parameter space for $N = 6, 8$ and 10 give plots as shown in FIG. 6. There exists a symmetry along $\tau_1 = \frac{\pi}{4}$, in the closed boundary condition but this symmetry is absent in the open boundary condition because in close chain Floquet system behavior of LMOTOC is same for Floquet period τ_1 and $\frac{\pi}{2} - \tau_1$, but in case of open chain both are not the same for long time. However, there is a symmetry about $\tau_0 = \frac{\pi}{4}$ in both the open and the closed chain [FIG. 4]. The tips of the regions with $\overline{F}_x = 0$ can be seen to be moving closer to each other with increasing the system size. In the open boundary condition, the tips which start out in the upper half of the parameter space, also move downwards towards the point $(\frac{\pi}{4}, \frac{\pi}{4})$ with increasing system size. For system size $N \rightarrow \infty$, we can expect the tips to meet at the centre, giving the critical lines as shown in FIG. 1, which is the expected phase diagram for this system. Hence, the time-averaged LMOTOC [$\overline{F}_x(T)$] for large T and $N \rightarrow \infty$ can be used as an order parameter to distinguish the phases of a driven transverse field Floquet Ising model. It must be noted that the time-averaged LMOTOC does not distinguish between the ferromagnetic and the π ferromagnetic phase or the paramagnetic and the 0π paramagnetic phase. However, these distinct phases can be identified by observing the combined eigenvalues of the unitary op-

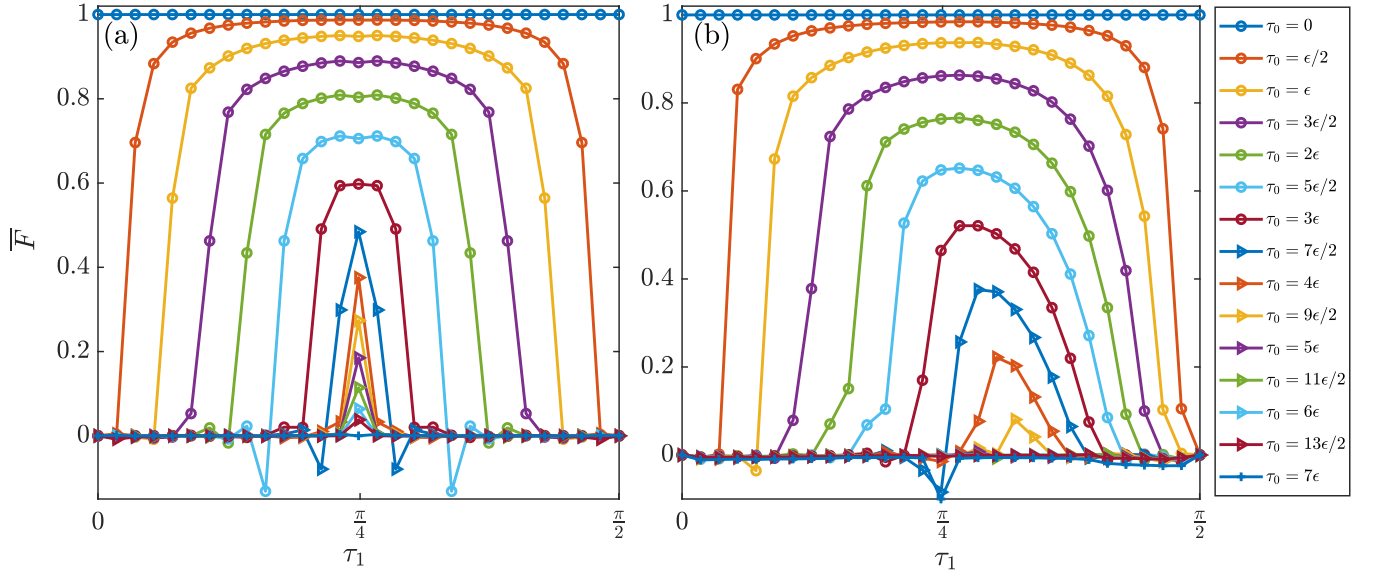


FIG. 5. Plot of $\bar{F}_x(T)$ with τ_1 for values of τ_0 varying from 0 to $\frac{\pi}{4}$ in intervals of ϵ in the (a) closed and (b) open chain Floquet systems of system size $N = 10$ and $T = 10^4$. The variation of $\bar{F}_x(T)$ with τ_1 for $\pi/4 < \tau_0 < \pi/2$ is the same as that for $\frac{\pi}{2} - \tau_0$. This plot can be used to find the regions in the τ_0 and τ_1 parameter space that have $\bar{F}_x(T) > 0$ and $\bar{F}_x(T) = 0$ (FIG. 6).

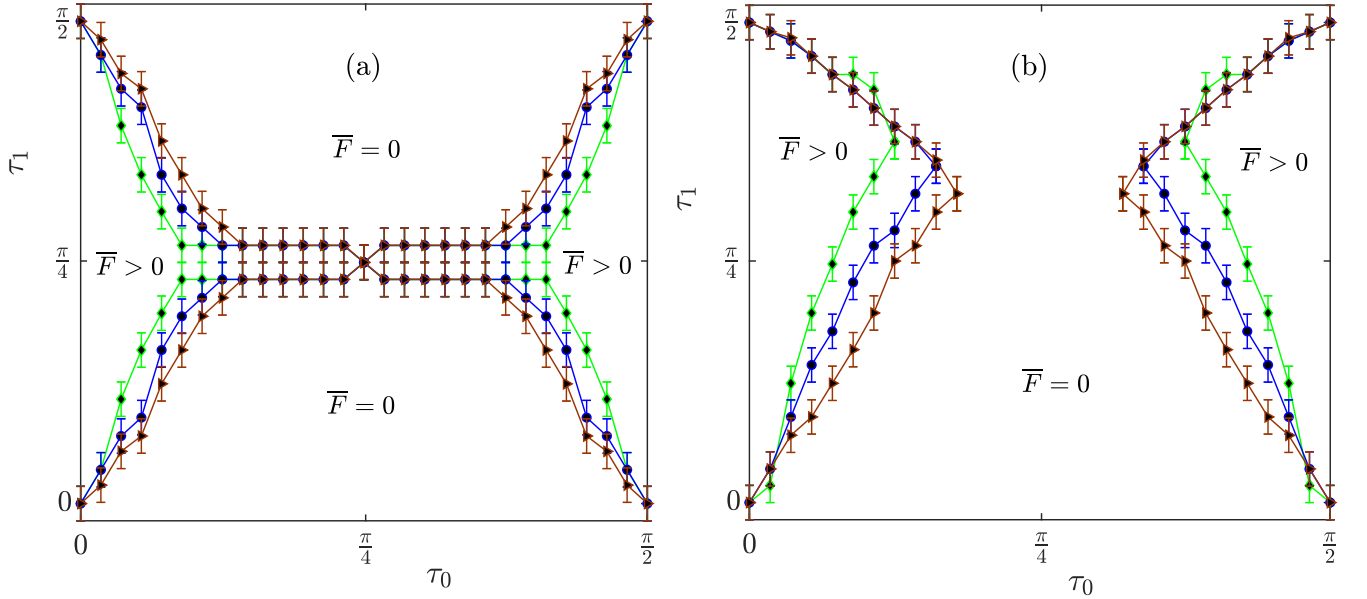


FIG. 6. Regions with $\bar{F}_x(T) > 0$ and $\bar{F}_x(T) = 0$ in the τ_0 and τ_1 parameter space with $T = 10^4$, for the (a) closed and (b) open chain Floquet systems of system size $N=6$ (Green), 8 (Blue) and 10 (Brown). As increasing system size, critical lines of both (a) and (b) tend towards diagonal critical lines. Hence, this suggests that the phase structure of the system would contain two ferromagnetic regions (where $\bar{F}_x > 0$) and two paramagnetic regions (where $\bar{F}_x = 0$).

erator which is defined in eq. (1) and the parity operator ($P = \prod_l \sigma_l^z$) [24, 27]. Considering the operators U and P have eigenvalues u and p respectively, the different phases can be distinguished by observing the eigenvalues along the outer edges of the phase diagram. The eigenvalues have protected multiplets of the form: (u, p) in the paramagnetic, $[(u, p), (u, -p), (-u, p), (-u, -p)]$ in

the 0π paramagnetic, $[(u, p), (u, -p)]$ in the ferromagnetic and $[(u, p), (-u, -p)]$ in the π ferromagnetic regions.

The frequencies of oscillations of the LMOTOC also provide a signature of the phase transitions. Here, the dominant frequencies have been numerically determined by taking the argument maxima of the discrete Fourier transforms of the deviation of the LMOTOC from its

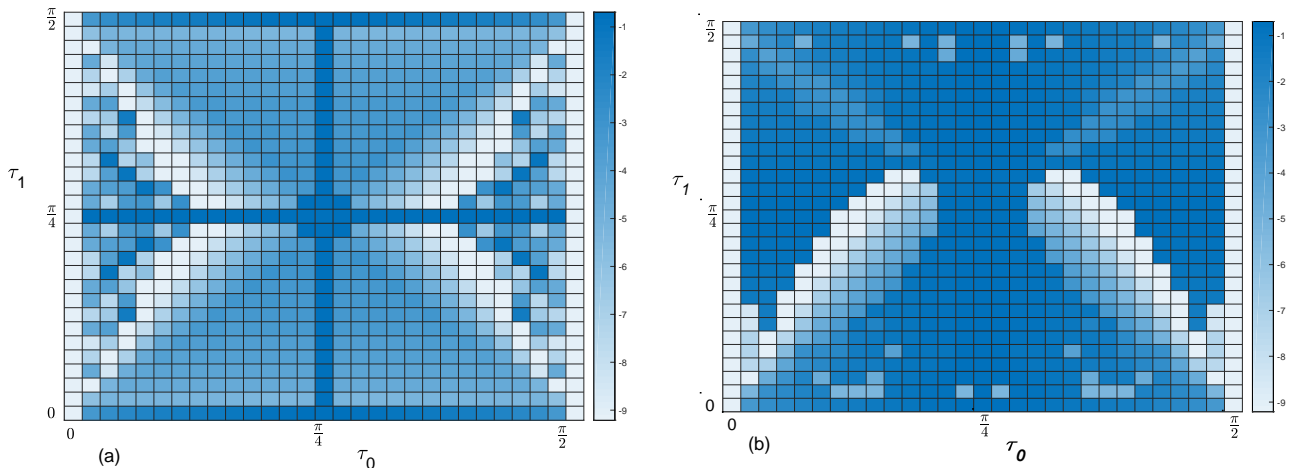


FIG. 7. Heat map of the logarithmic dominant frequencies of $F(n) - \bar{F}_x(T)$ in the discretized τ_0 - τ_1 parameter space for the (a) closed and (b) open Floquet system of system size $N = 10$ and with $T = 10^4$. The heat map shows logarithmically small values close to the transition lines shown in FIG. 6.

mean value ($F_x(n) - \bar{F}_x(T)$). Mathematically, it can be defined as:

$$\mathcal{F}(\nu) = \frac{1}{T} \sum_{n=1}^T [F_x(n) - \bar{F}_x(T)] e^{-i\frac{2\pi}{T}\nu n} \quad (15)$$

A heatmap of the dominant frequencies of $F(\nu)$ in the logarithmic scale is shown in FIG. 7 for $N = 10$ in the closed and open boundary conditions. These plots show that the dominant frequencies logarithmically drop close to the critical lines and at the edges. Comparing FIG. 7 and FIG. 6, we observe that heatmap displays indications of the phase transition in the Floquet Ising system.

V. CONCLUSION

We calculate the exact analytical expression for TMO-TOC as a function of τ_0 and τ_1 . Further, we study the phase structure of the traverse field Floquet Ising system given by eq. (1) using numerical calculation of LMO-TOC. We use LMOTOC defined in equation eq. (12) to distinguish between the paramagnetic and ferromagnetic phases of the chosen Floquet system. ferromagnetic and the π ferromagnetic phase or the paramagnetic and the 0π paramagnetic phase are distinguished by the combined eigenvalues of U and parity operator P . We numerically find the time averaged LMOTOC $[\bar{F}_x(T)]$ for the system sizes up to $N = 10$ and plot the regions of the parameter space that have $\bar{F}_x(T) = 0$ and $\bar{F}_x(T) > 0$ for $T = 10^4$. We observe that the plot showing the critical lines of phase transition for $N \rightarrow \infty$ tends to the expected plot FIG. 1.

In the limit $N \rightarrow \infty$, the regions with $\bar{F}_x(T) > 0$ for large T are ferromagnetic and those with $\bar{F}_x(T) = 0$ for large T are paramagnetic. We also see that the dominant

frequency of oscillations in $[F_x(n) - \bar{F}_x(T)]$ logarithmically decreases close to the critical line and the boundary of phase space for the system sizes considered.

OTOCs can be experimentally calculated [18], and Floquet systems can be experimentally realized [42, 43]. Our study outlines how LMOTOC can be a useful tool to distinguish the phases of a Floquet system.

VI. ACKNOWLEDGE

We would like to thank V. Subrahmanyam for his fruitful suggestion in the analytical calculation of TMOTOC.

Appendix A: Calculation of transverse magnetization OTOC

We transform the spin variables to fermionic creation c_l^\dagger and annihilation c_l operators at site l by using the Jordan-Wigner transformation [44]

$$S_l^x = -\frac{1}{2} \prod_{j=1}^{l-1} (2c_j^\dagger c_j - 1) (c_l^\dagger + c_l) \quad \text{and} \quad S_l^z = c_l^\dagger c_l - \frac{1}{2}. \quad (A1)$$

The operators c_l and c_l^\dagger obey the usual fermion anti-commutation rules. The unitary operator for the closed chain is given as

$$U = \exp \left[\frac{-it_1}{4} \left(\sum_{l=1}^{N-1} (c_l^\dagger - c_l) (c_{l+1}^\dagger - c_{l+1}) - (-1)^{N_F} (c_N^\dagger - c_N) (c_{l+1}^\dagger - c_{N+1}) \right) \right] \times \exp \left[-it_0 \sum_{l=1}^N (c_l^\dagger c_l - \frac{1}{2}) \right], \quad (A2)$$

where $N_F = \sum_{l=1}^L c_l^\dagger c_l$ is the total number of fermions. We move in the momentum space using the Fourier transform of c_l which is defined as

$$c_q = \frac{\exp(i\frac{\pi}{4})}{\sqrt{N}} \sum_{l=1}^N e^{-iq_l} c_l. \quad (\text{A3})$$

Hence U can be written as [45]

$$U = e^{(-it_0 \frac{N}{2})} \prod_{q>0} \mathcal{V}_q. \quad (\text{A4})$$

The operator \mathcal{V}_q in the above expression has the form

$$\mathcal{V}_q = \exp \left(-i \frac{t_1}{2} [\cos(q)(c_q^\dagger c_q + c_{-q}^\dagger c_{-q}) + \sin(q)(c_q c_{-q} + c_{-q}^\dagger c_q^\dagger)] \right) \exp \left(-2it_0(c_q^\dagger c_q + c_{-q}^\dagger c_{-q}) \right). \quad (\text{A5})$$

For \mathcal{V}_q , the four basis state are $|0\rangle$, $|\pm q\rangle = c_{\pm q}^\dagger |0\rangle$, $|-qq\rangle = c_{-q}^\dagger c_q^\dagger |0\rangle$

The eigenstates of \mathcal{V}_q are given by

$$\begin{aligned} \mathcal{V}_q |\pm q\rangle &= e^{(-\frac{t_1}{2} \cos(q) - it_0)} |\pm q\rangle, \\ \mathcal{V}_q |\pm\rangle &= e^{(-\frac{t_1}{2} \cos(q) - it_0)} e^{\pm i\gamma_q} |\pm\rangle, \end{aligned} \quad (\text{A6})$$

where

$$|\pm\rangle = \alpha_{\pm q} |0\rangle + \beta_{\pm q} |-qq\rangle. \quad (\text{A7})$$

In the above equation $\alpha_{\pm q}$ and $\beta_{\pm q}$ are given by eq. (10) and eq. (11) respectively. The initial unentangled state is $|\psi_L(0)\rangle = |0\rangle^{\otimes L}$. In Fock space, it is treated as vacuum. Time evolution operator of the fermionic annihilation operator in the momentum space is given as

$$c_q(n) = \mathcal{V}_q^{\dagger n} c_q \mathcal{V}_q^n = \Phi_q(n)^* c_q - \Psi_q(n) c_{-q}^\dagger. \quad (\text{A8})$$

The expansion coefficients $\Phi_q(n)$ and $\Psi_q(n)$ are defined in eq. (7) and eq. (8), respectively, and phase angle (γ_q)

is defined in eq. (9). Let us apply the first spin operator on the initial state, we get

$$S_l^z(0)|0\rangle = \left(c_l^\dagger c_l - \frac{1}{2} \right) |0\rangle = -\frac{1}{2} |0\rangle. \quad (\text{A9})$$

Since, $c_l^\dagger c_l$ is the number operator. The operation of the number operator on the vacuum gives zero eigenvalue. Time evolution of the spin operator at position l is

$$S_l^z(n) = \frac{1}{N} \sum_{a,b} e^{i(a-b)l} c_a^\dagger(n) c_b(n) - \frac{1}{2},$$

where a and b are indices in momentum space. By using eq. (A8), we can write

$$\begin{aligned} S_l^z(n) &= \frac{1}{N} \sum_{a,b} e^{i(a-b)l} \left[\Phi_a(n) c_a^\dagger - \Psi_a(n)^* c_{-a} \right] \\ &\quad \times \left[\Phi_b(n)^* c_b - \Psi_b(n) c_{-b}^\dagger \right] - \frac{1}{2}, \\ &= \frac{1}{N} \sum_{a,b} e^{i(a-b)l} \left[\Phi_a(n) \Phi_b(n)^* c_a^\dagger c_b - \Phi_a(n) \Psi_b(n) c_a^\dagger c_{-b}^\dagger \right. \\ &\quad \left. - \Psi_a(n) \Phi_b(n)^* c_{-a} c_b + \Psi_a(n)^* \Psi_b(n) c_{-a} c_{-b}^\dagger \right] - \frac{1}{2}, \end{aligned} \quad (\text{A10})$$

Application of time evolved spin operator on the vacuum gives

$$\begin{aligned} S_l^z(n)|0\rangle &= \left[-\frac{1}{N} \sum_{a,b} e^{i(a-b)l} \Phi_a(n) \Psi_b(n) c_a^\dagger c_{-b}^\dagger \right. \\ &\quad \left. + \frac{1}{N} \sum_a |\Psi_a(n)|^2 - \frac{1}{2} \right] |0\rangle, \end{aligned} \quad (\text{A11})$$

and the Hermitian conjugate of the above equation is

$$\begin{aligned} \langle 0 | S_l^z(n) &= \langle 0 | \left[-\frac{1}{N} \sum_{p,r} e^{-i(p-r)l} \Phi_p(n)^* \Psi_r(n)^* c_{-r} c_p \right. \\ &\quad \left. + \frac{1}{N} \sum_p |\Psi_p(n)|^2 - \frac{1}{2} \right], \end{aligned} \quad (\text{A12})$$

where p and r are indices in the momentum space. We can calculate $S_l^z(n) S_l^z(0) |0\rangle$ as

$$\begin{aligned} S_l^z(n) S_l^z(0) |0\rangle &= -\frac{1}{2} \left[-\frac{1}{N} \sum_{a,b} e^{i(a-b)l} \Phi_a(n) \Psi_b(n) c_a^\dagger c_{-b}^\dagger \right. \\ &\quad \left. + \frac{1}{N} \sum_a |\Psi_a(n)|^2 - \frac{1}{2} \right] |0\rangle. \end{aligned} \quad (\text{A13})$$

Applying the third spin operator $S_l^z(0)$ on the state $S_l^z(n)S_l^z(0)|0\rangle$ we get

$$\begin{aligned}
S_l^z(0)S_l^z(n)S_l^z(0)|0\rangle &= -\frac{1}{2}\left[\frac{1}{N}\sum_{x,y}e^{i(x-y)l}c_x^\dagger c_y - \frac{1}{2}\right]\left[-\frac{1}{N}\sum_{a,b}e^{i(a-b)l}\Phi_a(n)\Psi_b(n)c_a^\dagger c_{-b}^\dagger + \frac{1}{N}\sum_a|\Psi_a(n)|^2 - \frac{1}{2}\right]|0\rangle, \\
&= -\frac{1}{2}\left[-\frac{1}{N^2}\sum_{x,y,a,b}e^{i(x-y)l}e^{i(a-b)l}\Phi_a(n)\Psi_b(n)\left(c_x^\dagger c_{-b}^\dagger\delta(a,y) - c_x^\dagger c_a^\dagger\delta(-b,y)\right)\right. \\
&\quad \left. + \frac{1}{2N}\sum_{a,b}e^{i(a-b)l}\Phi_a(n)\Psi_b(n)c_a^\dagger c_{-b}^\dagger - \frac{1}{2}\left(\frac{1}{N}\sum_a|\Psi_a(n)|^2 - \frac{1}{2}\right)\right]|0\rangle, \tag{A14}
\end{aligned}$$

where x and y are the indices in the momentum space. Now we take the scalar product of the states given by eq. (A12) and eq. (A14) and get TMOTOC as

$$\begin{aligned}
F_z(n) &= 2^4\langle 0|S_l^z(n)S_l^z(0)S_l^z(n)S_l^z(0)|0\rangle, \\
&= -2^3\langle 0|\left[-\frac{1}{N}\sum_{p,r}e^{-i(p-r)l}\Phi_p(n)^*\Psi_r(n)^*c_{-r}c_p + \frac{1}{N}\sum_p|\Psi_p(n)|^2 - \frac{1}{2}\right]\left[-\frac{1}{N^2}\sum_{x,y,a,b}e^{i(x-y)l}e^{i(a-b)l}\Phi_a(n)\right. \\
&\quad \left.\times\Psi_b(n)\left(c_x^\dagger c_{-b}^\dagger\delta(a,y) - c_x^\dagger c_a^\dagger\delta(-b,y)\right) + \frac{1}{2N}\sum_{a,b}e^{i(a-b)l}\Phi_a(n)\Psi_b(n)c_a^\dagger c_{-b}^\dagger - \frac{1}{2}\left(\frac{1}{N}\sum_a|\Psi_a(n)|^2 - \frac{1}{2}\right)\right]|0\rangle, \\
&= -2^3\left[\frac{1}{N^3}\left(\sum_{p,a,r}|\Psi_r(n)|^2\Phi_p^*(n)\Phi_a(n) - \Psi_{-p}(n)\Psi_r(n)^*\Phi_p^*(n)\Phi_a(n) - \Psi_a(n)\Psi_r(n)^*\Phi_p(n)^*\Phi_{-r}(n) + \Psi_a(n)\right.\right. \\
&\quad \left.\left.\times\Psi_r(n)^*|\Phi_p(n)|^2\right) - \frac{1}{2N^2}\sum_{p,r}\left(|\Psi_p(n)|^2|\Phi_r(n)|^2 - \Psi_{-p}(n)\Psi_r(n)^*\Phi_p(n)^*\Phi_{-r}(n)\right)\right. \\
&\quad \left.- \frac{1}{2}\left(\frac{1}{N}\sum_p|\Psi_p(n)|^2 - \frac{1}{2}\right)\left(\frac{1}{N}\sum_a|\Psi_a(n)|^2 - \frac{1}{2}\right)\right]. \tag{A15}
\end{aligned}$$

Since, the term

$$\frac{1}{2N^2}\sum_{p,r}\left(|\Psi_p(n)|^2|\Phi_r(n)|^2 - \Psi_{-p}(n)\Psi_r(n)^*\Phi_p(n)^*\Phi_{-r}(n)\right) + \frac{1}{2}\left(\frac{1}{N}\sum_p|\Psi_p(n)|^2 - \frac{1}{2}\right)\left(\frac{1}{N}\sum_a|\Psi_a(n)|^2 - \frac{1}{2}\right) \tag{A16}$$

is constant for all number of kicks (n) and system size (N) which comes out to be $\frac{1}{2^3}$. Since a is a dummy index, we replace it by q . Hence, the final formula of TMOTOC is

$$\begin{aligned}
F_z(n) &= 1 - \left(\frac{2}{N}\right)^3\sum_{p,q,r}\left(|\Psi_r(n)|^2\Phi_p^*(n)\Phi_q(n) - \Psi_{-p}(n)\Psi_r(n)^*\Phi_p^*(n)\Phi_q(n)\right. \\
&\quad \left.- \Psi_q(n)\Psi_r(n)^*\Phi_p(n)^*\Phi_{-r}(n) + \Psi_q(n)\Psi_r(n)^*|\Phi_p(n)|^2\right). \tag{A17}
\end{aligned}$$

[1] S. Ray, S. Sinha, and K. Sengupta, Phys. Rev. A **98**, 053631 (2018).
[2] P. Hosur, X.-L. Qi, D. A. Roberts, and B. Yoshida, Journal of High Energy Physics **2016**, 4 (2016).
[3] Y. Gu and X.-L. Qi, Journal of High Energy Physics **2016**, 129 (2016).
[4] Y. Ling, P. Liu, and J.-P. Wu, Journal of High Energy Physics **2017**, 25 (2017).
[5] A. Bohrdt, C. B. Mendl, M. Endres, and M. Knap, New Journal of Physics **19**, 063001 (2017).
[6] B. Swingle and N. Y. Yao, Physics **10**, 82 (2017).
[7] B. Swingle, G. Bentsen, M. Schleier-Smith, and P. Hayden,

Phys. Rev. A **94**, 040302 (2016).
[8] B. Swingle and D. Chowdhury, Phys. Rev. B **95**, 060201 (2017).
[9] M. Schleier-Smith, Nature Physics **13**, 724 (2017).
[10] S. Pappalardi, A. Russomanno, B. Žunkovič, F. Iemini, A. Silva, and R. Fazio, Phys. Rev. B **98**, 134303 (2018).
[11] M. J. Klug, M. S. Scheurer, and J. Schmalian, Phys. Rev. B **98**, 045102 (2018).
[12] V. Khemani, A. Vishwanath, and D. A. Huse, Phys. Rev. X **8**, 031057 (2018).
[13] Y. Alavirad and A. Lavasani, Phys. Rev. A **99**, 043602 (2019).

- [14] J. Maldacena, S. H. Shenker, and D. Stanford, *Journal of High Energy Physics* **2016**, 106 (2016).
- [15] S. H. Shenker and D. Stanford, *Journal of High Energy Physics* **2014**, 67 (2014).
- [16] D. A. Roberts, D. Stanford, and L. Susskind, *Journal of High Energy Physics* **2015**, 51 (2015).
- [17] M. Grtner, J. G. Bohnet, A. Safavi-Naini, M. L. Wall, J. J. Bollinger, and A. M. Rey, *Nature Physics* **13**, 781786 (2017).
- [18] J. Li, R. Fan, H. Wang, B. Ye, B. Zeng, H. Zhai, X. Peng, and J. Du, *Phys. Rev. X* **7**, 031011 (2017).
- [19] H. Shen, P. Zhang, R. Fan, and H. Zhai, *Phys. Rev. B* **96**, 054503 (2017).
- [20] Z.-H. Sun, J.-Q. Cai, Q.-C. Tang, Y. Hu, and H. Fan, arXiv preprint arXiv:1811.11191 (2018).
- [21] M. Heyl, F. Pollmann, and B. Dóra, *Phys. Rev. Lett.* **121**, 016801 (2018).
- [22] M. Heyl, A. Polkovnikov, and S. Kehrein, *Phys. Rev. Lett.* **110**, 135704 (2013).
- [23] F. Pollmann, A. M. Turner, E. Berg, and M. Oshikawa, *Phys. Rev. B* **81**, 064439 (2010).
- [24] C. W. von Keyserlingk and S. L. Sondhi, *Phys. Rev. B* **93**, 245145 (2016).
- [25] M. Thakurathi, A. A. Patel, D. Sen, and A. Dutta, *Phys. Rev. B* **88**, 155133 (2013).
- [26] A. M. Turner, F. Pollmann, and E. Berg, *Phys. Rev. B* **83**, 075102 (2011).
- [27] C. W. von Keyserlingk and S. L. Sondhi, *Phys. Rev. B* **93**, 245146 (2016).
- [28] X.-y. Feng, G.-m. Zhang, and T. Xiang, *Phys. Rev. Lett.* **98**, 087204 (2007).
- [29] V. M. Bastidas, C. Emary, G. Schaller, and T. Brandes, *Phys. Rev. A* **86**, 063627 (2012).
- [30] L. Jiang, T. Kitagawa, J. Alicea, A. R. Akhmerov, D. Pekker, G. Refael, J. I. Cirac, E. Demler, M. D. Lukin, and P. Zoller, *Phys. Rev. Lett.* **106**, 220402 (2011).
- [31] L. Fidkowski and A. Kitaev, *Phys. Rev. B* **83**, 075103 (2011).
- [32] V. Khemani, A. Lazarides, R. Moessner, and S. L. Sondhi, *Phys. Rev. Lett.* **116**, 250401 (2016).
- [33] M. Thakurathi, K. Sengupta, and D. Sen, *Phys. Rev. B* **89**, 235434 (2014).
- [34] B. K. Chakrabarti, A. Dutta, and P. Sen, *Quantum Ising phases and transitions in transverse Ising models*, Vol. 41 (Springer Science & Business Media, 2008).
- [35] S.-Q. Su, J.-L. Song, and S.-J. Gu, *Phys. Rev. A* **74**, 032308 (2006).
- [36] K.-W. Sun and Q.-H. Chen, *Physical Review B* **80**, 174417 (2009).
- [37] S. A. Parameswaran, A. C. Potter, and R. Vasseur, *Annalen der Physik* **529**, 1600302 (2017).
- [38] L. Zhang, V. Khemani, and D. A. Huse, *Physical Review B* **94**, 224202 (2016).
- [39] F. H. L. Essler, S. Evangelisti, and M. Fagotti, *Phys. Rev. Lett.* **109**, 247206 (2012).
- [40] R. de Mello Koch, J.-H. Huang, C.-T. Ma, and H. J. Van Zyl, *Physics Letters B* **795**, 183 (2019).
- [41] E. Dyer and G. Gur-Ari, *Journal of High Energy Physics* **2017**, 75 (2017).
- [42] M. S. Allen (*American Society of Mechanical Engineers*, 2007) pp. 823–833.
- [43] M. Chitsazi, H. Li, F. M. Ellis, and T. Kottos, *Phys. Rev. Lett.* **119**, 093901 (2017).
- [44] P. Jordan and E. Wigner, *Z. Phys.* **47**, 631 (1928).
- [45] A. Lakshminarayan and V. Subrahmanyam, *Phys. Rev. A* **71**, 062334 (2005).